ASME Journal of Vibration and Acoustics
Online journal at:
https://asmedigitalcollection.asme.org/vibrationacoustics

Zhenkun Guo
College of Mechatronics and Vehicle Engineering,
Beijing Key Laboratory of Performance Guarantee on Urban Rail Transit Vehicles;
Beijing University of Civil Engineering and Architecture,
Beijing 100044, China
e-mail: guozhenkun@bucea.edu.cn

Jiaqi Wen
College of Mechatronics and Vehicle Engineering,
Beijing Key Laboratory of Performance Guarantee on Urban Rail Transit Vehicles;
Beijing University of Civil Engineering and Architecture,
Beijing 100044, China
e-mail: wenjq98@163.com

Dewen Yu
School of Mechanical Engineering,
Key Laboratory of Modern Design and Rotor-Bearing System (Ministry of Education);
Xi'an Jiaotong University,
Xi'an 710049, China
e-mail: n2107433e@e.ntu.edu.sg

Guobiao Hu[1]
Internet of Things Thrust,
The Hong Kong University of Science and Technology (Guangzhou),
Guangzhou 511400, China
e-mail: guobiaohu@hkust-gz.edu.cn

Yaowen Yang
School of Civil and Environmental Engineering,
Nanyang Technological University,
Singapore 639798
e-mail: cywyang@ntu.edu.sg

Widening the Band Gaps of Hourglass Lattice Truss Core Sandwich Structures for Broadband Vibration Suppression

This paper proposes a novel phononic crystal sandwich beam (PCSB) for low-frequency and broadband vibration suppression. The representative volume element (RVE) consists of two hourglass truss unit cells with the same span but different rod radii. After validating the modeling method, a model of the PCSB is established to calculate band structure and transmittance response, and the results show good agreement. It is found that the PCSB can open wider and lower band gaps compared to a traditional sandwich beam (TSB). The band-folding mechanism is applied. The PCSB breaks the spatial symmetry, becomes diatomic, and opens the folding points, finally leading to two band-folding-induced gaps. The experiment is conducted on the PCSB, and the vibration band gap property is confirmed. Subsequently, the impacts of geometric parameters on the PCSB's band gaps are investigated in detail. Design guidelines for tuning the geometric parameters toward lower frequency and broadband band gap are provided based on the parametric study results. In addition, the higher-order band-folding strategy is proposed. It is shown that a multi-folding PCSB can produce more band gaps. However, through two examples, i.e., second-folding and third-folding PCSBs, it is known that simply increasing the folding order may not be effective and even could deteriorate the vibration attenuation ability. In summary, this work explores a general strategy for designing sandwich beams with low-frequency and broadband vibration suppression ability.
[DOI: 10.1115/1.4063443]

Keywords: phononic crystal, sandwich beam, band gap, broadband vibration suppression, band-folding, dynamics, structural dynamics and control, vibration isolation

1 Introduction

Ultralight porous sandwich structures have attracted enormous attention due to their superior properties, such as high stiffness/strength-to-weight ratios [1] and multifunctional characteristics [2]. Multiple sandwich structures have many engineering applications, particularly in the aerospace and marine fields, where structural weights are strictly limited. In recent decades, numerous studies have been reported on topology optimization, advanced fabrication techniques, and dynamic/static mechanical analyses of various sandwich structures with different lattices [2–6]. Extraordinary properties, such as heat transfer performance [7], high-impact resistance [8], and electromagnetic wave absorption [9], of some lightweight sandwich structures, have been revealed and validated. However, sandwich structures are susceptible and less resilient to vibrations because of their lightweight characteristics. Researchers have not fully unveiled the vibro-acoustic mechanism of lightweight sandwich structures, and related theoretical and experimental research keeps emerging. Traditional passive vibration attenuation strategies often require devices to have larger or near-wavelength volumes, especially for low-frequency vibrations [10]. Designing sandwich structures for low-frequency vibration suppression is a meaningful but, at the same time, challenging problem.

Over the past decades, new ways have been developed to mitigate low-frequency vibrations in lightweight structures. Metamaterials typically consist of mechanical host structures with periodically embedded or connected local resonators. Due to the local resonance

[1]Corresponding author.

Contributed by the Technical Committee on Vibration and Sound of ASME for publication in the Journal of Vibration and Acoustics. Manuscript received May 7, 2023; final manuscript received September 3, 2023; published online October 6, 2023. Assoc. Editor: Julien Meaud.

(LR) mechanism, wave propagation is prohibited in frequency ranges, i.e., band gaps [11,12]. Owing to this unique phenomenon, the investigation of metamaterial theory and its applications in vibration attenuation has attracted extensive research interest. Bragg scattering (BS) [13] is one of the two main mechanisms of band gap generation, and the other is LR [14]. The BS and LR mechanisms are different, but they can transform into each other under certain conditions and by varying the system parameters. Liu and Hussein [15] presented a comprehensive study and characterized the condition for the transition between BS and LR. The former exists in phononic crystals (PCs), and the wave in the structure will be affected by the periodic scatterers. When the wavelength and the lattice constant are the same order, a band gap will be generated in this range. To effectively attenuate low-frequency waves, a large lattice constant is required. However, such a requirement is not feasible in many engineering structures. Unlike PCs, producing low-frequency band gap is the characteristic of the LR mechanism. Therefore, significant efforts have been dedicated to study and manipulation of LR band gaps, such as how to broaden bandwidth, so as to meet the vibration reduction requirements in complex engineering environments [16–18].

The lattice structures designed in most previous studies for producing band gaps share a common feature: local resonators are inserted into periodic cells of the host structure to achieve LR band gaps. The bending vibration of the sandwich beam that featured local resonators integrated within the foam core layer was studied by Chen and Sun [19]. Their assumption was that the resonators were evenly spaced along the beam, and they developed an analytical model using the volume average approach. However, they did not consider how to really implement practical local resonators in the sandwich beams. Sharma and Sun [20] calculated the propagation constant of a sandwich beam with resonators inserted in the core layer using a phased array approach. They explained the periodicity effect of the resonator on bending vibration. Instead of embedding additional mass-spring oscillators, Guo et al. [21] proposed a novel metamaterial sandwich beam with hourglass cores. In their proposed model, concentrated masses were added at the intersections of slanted struts in the hourglass core to realize low-frequency local resonators. The slanted struts serve as elastic stiffness in the transverse direction and play the role of springs. Based on a similar idea, Li et al. [22] fabricated the specimen of sandwich metamaterial plates using 3D printing technology and validated the low-frequency vibration suppression performance via experimental studies. Furthermore, Guo et al. [23] proposed a lattice truss core sandwich metastructure with the BS-LR coupling effect. To facilitate the dynamics of the metastructure and prediction of the band gap, they developed an efficient multiscale modeling approach by utilizing the dynamic homogenization method and spectral element method. An et al. [24] proposed a meta-orthogrid sandwich plate (MOSP) and studied the vibration transmittance through simulations and experiments. An analysis was conducted on how changes to the core layer affect the vibration transmittance of the lower and upper faceplates of the MOSP. Furthermore, nonlinear resonant oscillators can generate ultra-low-frequency band gaps [25,26]. Xue et al. [27] designed a simple metamaterial sandwich structure in which the resonant oscillator was composed of a buckling beam and a lumped mass fixed at the free end. This kind of oscillator can effectively lower the band gap frequency by generating nonlinearity, compared with linear ones [28]. However, this proposed structure should not be deemed a sandwich structure in the strict sense since the designer changed the host structure, and it is more appropriate to be referred to as a dual-beam structure [29,30]. According to the literature review, LR sandwich metamaterials/metastructures require engineered oscillators in the core layers. Such design may cause problems: (1) The embedded oscillators complicate the structures and increase the manufacturing difficulty and cost. (2) If only small and lightweight oscillators are allowed, the produced band gaps will be very narrow, especially in the low-frequency range. If heavy oscillators are added, the lightweight advantage will be deteriorated, limiting the wide-ranging application scenarios for sandwich structures.

Hourglass lattice truss core sandwich structures outperform traditional core sandwich structures in terms of static properties [31,32]. However, their dynamic properties and band gap behaviors are less researched. This article proposes a novel phononic crystal sandwich beam (PCSB) to achieve more favorable band gap characteristics. The PCSB's alternately changing hourglass truss cores can produce BS band gap. The representative volume element (RVE) contains two adjacent unit cells with the same span but different rod radii. The finite element (FE) model is built, and the dispersion relation is predicted. Moreover, the vibration transmittance is also calculated. Two low-frequency band gaps can be generated in the PCSB compared with the traditional sandwich beam (TSB). The behind band-folding mechanism is explained. The experiment achieves the expected results. Finally, the impact of structural parameters and band-folding times of the PCSB are studied.

2 Modeling and Verification

Figure 1 shows the TSB with the hourglass lattice truss core composed of three-layer construction, i.e., a soft core layer consisted of inclined rods with small equivalent mass density connects the upper and bottom face sheets [32]. The TSB exhibits periodicity in the axial direction. According to the theory of PC, the periodicity can induce the BS effect and thus produce BS band gaps for forbidding the wave propagation over these ranges. However, as mentioned above, due to the structure size limitation, realizing broad and low-frequency band gaps is challenging, which restricts the application of sandwich structures in an environment with vibrations spreading over a wide spectrum.

To broaden bandwidth of TSB, a novel PCSB is developed by employing the band-folding strategy [33,34]. Figure 2(*a*) shows the RVE that constitutes the TSB. As Fig. 2(*b*) shows, the RVE

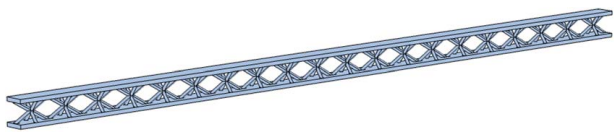

Fig. 1 Diagram of the TSB with hourglass lattice truss core

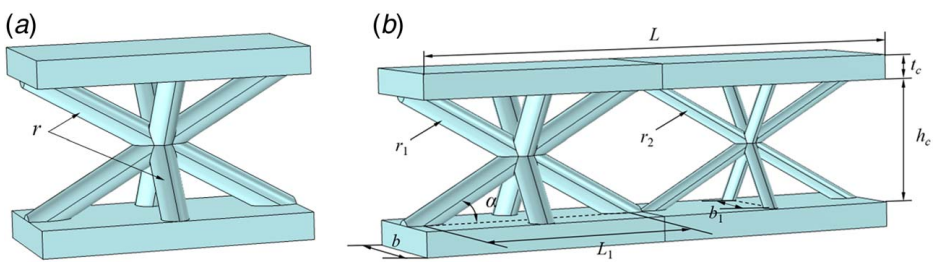

Fig. 2 (*a*) Unit cell of the TSB and (*b*) RVE of the PCSB

of the PCSB consists of two subcells with identical span. The radii of the strut rods in the two adjacent unit cells are different, i.e., $r_1 \neq r_2$.

We first validate our modeling method by repeating the study of a pyramidal truss core sandwich beam in the literature [35], and the parameters are taken from the original paper [35]. The sandwich beam is cantilevered, i.e., both ends are clamped and free. The natural frequencies and mode shapes of the pyramidal truss core sandwich beam are extracted by simulation, and the proposed method and by Lou et al. [35] are compared in Table 1 through. Only a minor relative error is observed, validating the accuracy of the present modeling approach. Additionally, the corresponding vibration modes of the model are plotted in Fig. 3. The displacement contour plot shows that the clamped end exhibits small displacement since the clamped constraint condition takes effect. Therefore, the modeling process of sandwich beams in this paper is reasonable and can be used in succedent research.

Subsequently, the RVE of the PCSB, as shown in Fig. 2(*b*), is modeled using COMSOL. The geometric parameters and material properties are listed in Table 2. L denotes the span of the RVE; b denotes the width; r_1 and r_2 denote the rod radii of the hourglass trusses in the left and right unit cells; h_c denotes the thickness of the core layer; t_c denotes the thickness of the upper and bottom face sheets; and α denotes the inclination angle of the rod. The length and width of the projection of the rods on the face sheets are $L_1 = h_c/(2\tan\alpha)$ and $b_1 = 0.75b$, respectively.

3 Structural Dynamic Analysis

In this section, the simulation analysis of the PCSB is focused on. The band gaps are predicted by the dispersion relation analysis and verified by the vibration transmittance analysis. When Bragg scattering occurs in wave propagation in periodic structures, incident and reflected waves superpose, forming constructive and destructive interferences, resulting in the band gap. The frequency domain response, also known as transmittance, is defined as the ratio of the unconstrained end displacement to the base excitation displacement. When the displacement response at the unconstrained end is smaller than the base excitation, the transmittance value in the decibel scale is smaller than 0, and the transmittance curve appears as a valley.

Table 1 Comparison of natural frequencies (Hz) of the pyramidal sandwich beam calculated using different methods

Modes	Present method	Lou et al. [35]	Relative error
1	44.389	43.468	2.12%
2	268.81	265.01	1.43%
3	713.62	712.04	0.22%
4	1297.8	1321.2	1.77%
5	1954.7	2051.8	4.73%

3.1 Band Structure Analysis. The Bloch–Floquet periodic boundary conditions are imposed to the RVE in COMSOL, and the dispersion relationship of the infinitely long PCSB can be obtained. As shown in the band structure in Fig. 4, three frequency ranges (1530.33–2149.04 Hz, 3419.87–3685.86 Hz, and 6535.85–6615.90 Hz) appear within 0–8000 Hz. In comparison, the dispersion curves of the TSB with $r = 5$ mm are also plotted out as shown in Fig. 5. It is found that the TSB produces only one band gap below 8000 Hz, and the specific frequency range is about 4158.83–5223.69 Hz. The PCSB induces two more band gaps than the TSB, and the first two move to the lower frequencies. This is because as the rod radius of the hourglass truss in the right unit cell reduces from 5 to 3 mm, the equivalent stiffness of the RVE becomes smaller. Consequently, this decreases the global bending stiffness, thus lowering the structural frequencies and bringing desirable band gaps. Although the total bandwidth (the sum of the three band gap widths) does not increase, realizing a significantly lower frequency band gap is favorable.

3.2 Transmittance Analysis. As shown in Fig. 6, to verify the band gap properties of the PCSB in the previous section, a PCSB containing 20 RVEs is considered and analyzed. The left end is clamped and mounted to a shaking block with a harmonic excitation prescribed base excitation in the specified z-direction. The displacement responses at both ends are measured, and the ratio of two is obtained and processed logarithmically to obtain the transmittance curve. The transmittance function Γ_{re} is defined as [36]

$$\Gamma_{re} = 20 \cdot \log_{10} \frac{d_{\text{free-end}}}{d_{\text{excitation}}}$$

where $d_{\text{exicition}}$ and $d_{\text{free-end}}$ are the input excitation and the displacement at the free end in the z-direction, respectively. Γ_{re} is positive, i.e., greater than 0, when the displacement of the beam free end is larger than that of base excitation, indicating the beam vibration is amplified. In contrast, Γ_{re} is negative, i.e., less than 0, when the displacement of the beam free end is smaller than that of base excitation, indicating the beam vibration is suppressed.

Figure 7(*b*) shows that the transmittance indicates the existence of band gaps over the frequency ranges 1530–2180 Hz and 3440–3720 Hz, which are consistent with those in band structure analysis in Fig. 7(*a*). The band structure and transmittance analyses have mutually verified each other. When the displacement at the unconstrained end is smaller than the input excitation, the transmittance in the decibel scale appears to be negative. Valleys form over the ranges with negative transmittance values, indicating a vibration

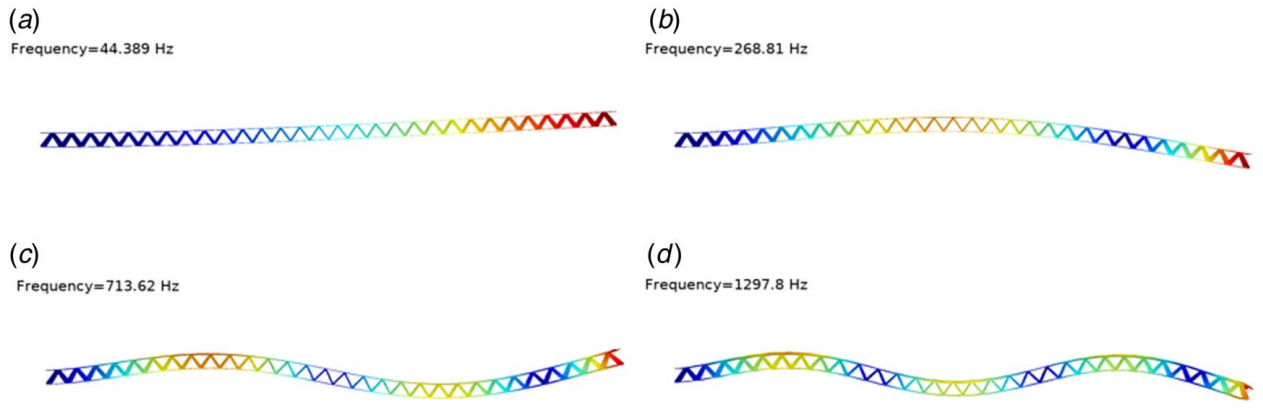

Fig. 3 Vibration modes of the pyramidal sandwich beam: (*a*) first mode, (*b*) second mode, (c) third mode, and (*d*) fourth mode

Table 2 The geometric and material parameters of the PCSB

L (mm)	b (mm)	r_1 (mm)	r_2 (mm)	h_c (mm)	t_c (mm)	L_1 (mm)	E (GPa)	ρ (kg/m^3)	ν
200	50	5	3	50	10	87.5	200	7850	0.3

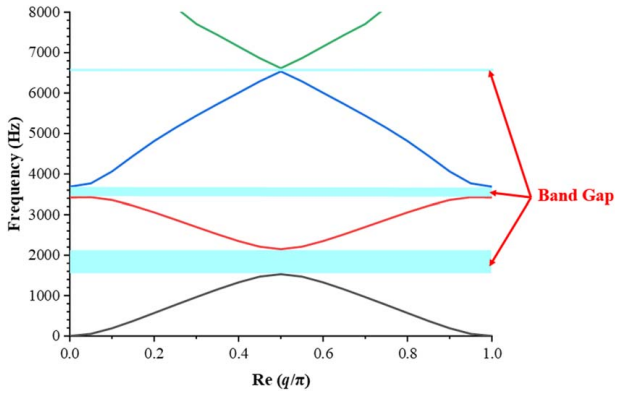

Fig. 4 Band structure of the PCSB

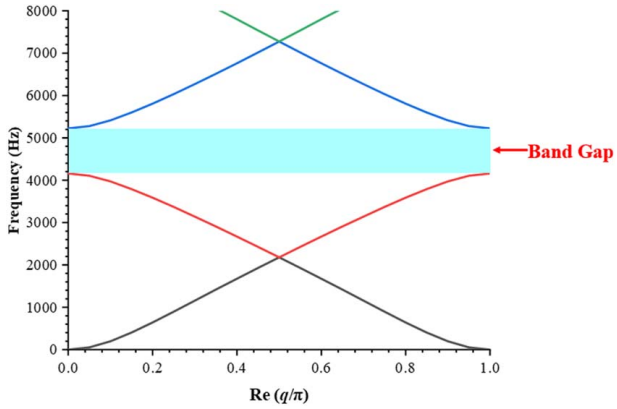

Fig. 5 Band structure of the TSB

Fig. 6 A finitely long PCSB containing 20 RVEs under the base excitation

attenuation effect. The smaller the transmittance, the more significant the attenuation effect is. To help further understand the characteristics of the band gap, several specific vibration modes are plotted in Fig. 8.

Figures 8(*a*) and 8(*b*) are the vibration modes in band gaps at 1830 Hz and 3650 Hz, respectively. Figure 8(*c*) is the vibration mode at 5160 Hz, which is out of the two band gaps. It is observed that the bending deformation dramatically decreases along the length direction of the PCSB in the band gaps. Unsurprisingly, obvious deformation exists near the unconstrained end when the excitation frequency is out of these ranges. The vibration mode analysis results have firmly confirmed the vibration attenuation capability of the PCSB.

3.3 Band-Folding Effect. In the previous section of the research process, we noticed that after simply doubling the unit cell size, a cone-like dispersion relation appeared in the diatomic metamaterial, known as the Dirac cone [34]. We then introduce diversity into the diatomic metamaterial by making the left and right cells have different trusses, the band-folding points are opened, and new band gaps are generated. Band-folding is actually a common phenomenon for superlattices in PCs. As an example, the simple cubic of an atom with lattice parameter a is shown in Fig. 9(*a*). Based on the correspondence between the space basis vectors a_1, a_2, a_3 and the inverse lattice basis vectors b_1, b_2, b_3 [37], its inverse lattice is a cube, and its side length is $2\pi/a$ as plotted in Fig. 9(*c*). If one double-volume cell is taken, its inverse space becomes a cuboid, as shown in Fig. 9(*b*). According to the correspondence between the real space and inverse space, the volume of inverse space reduces by half, and the basis vector in the k_x-direction reduces by half, as shown in Fig. 9(*d*). Hence, ΓX is twice large as Γ_1X_1 in the k_x-direction.

The band structure of the TSB for which RVE consists of one unit cell is calculated, as shown in Fig. 2(*a*), as well as the band structure of a double-sized RVE with two identical TSB unit cells. The difference is whether one unit or two units of the periodic structure are taken in calculating the band structure. Compared with one unit cell, the Brillouin zone of RVE consists of two identical unit cells and is reduced to half, given the geometrical parameters are kept the same. Consequently, the dispersion curve is folded along the midline (ΓX) of the Brillouin zone. The bottom band of the wave vector from 0 to 0.5 in Fig. 10(*a*) corresponds to the band below the folding point in Fig. 10(*b*), while the remaining right half goes to the next cell. Based on the Bloch theorem, the physical properties at a position in the next cell are the same as the corresponding position in this cell, and the relationship between wave vector and energy is the same. Finally, the band above the folding point in Fig. 10(*b*) is formed.

In Fig. 10(*b*), we notice the folding point at the intersection of the dispersion curves. It is like a Dirac cone that occurs at the cross-over of two linear dispersion curves at the corners of the Brillouin zone. Dirac points often occur at the K and Γ points of the Brillouin zone. Indaleeb et al. [38,39] demonstrated multiple occurrences of Dirac-like cones through numerical and experimental studies of a baseline periodic structure having a square array of cylindrical polyvinylchloride inclusions in an air matrix. The Dirac point is generated due to accidental degeneracy at the predicted frequency. He et al. [40] used a three-dimensional topological acoustic crystal with pseudospins using bilayer chiral structures to generate multi-level topological band gaps. They found that if the system symmetry is destroyed, the Dirac point will annihilate and split the degeneracy. The band crossing point formed by the band-folding is referred to as a folding point [34]. Breaking spatial symmetry, such as the PCSB given in Fig. 2(*b*), opens the folding points and generates two new band gaps. This could be helpful for realizing broadband vibration suppression. In Fig. 4, the top and bottom band gaps in PCSB originate from the opening of folding points, while the middle band gap is inherited from the TSB.

3.4 Experimental Investigation. For the PCSB designed in this paper, relevant experiments were conducted to verify the previous simulation results in this section, including the production of experimental samples, process, and results.

Due to the internal complexity of PCSB and the limitation of manufacturing technology in metal materials, the beam material used in this section is polylactic acid (PLA), and the geometric parameters and material properties are given in Table 3.

The model of the PCSB is made in SOLIDWORKS software and then saved as an STL file. With the help of additive manufacturing

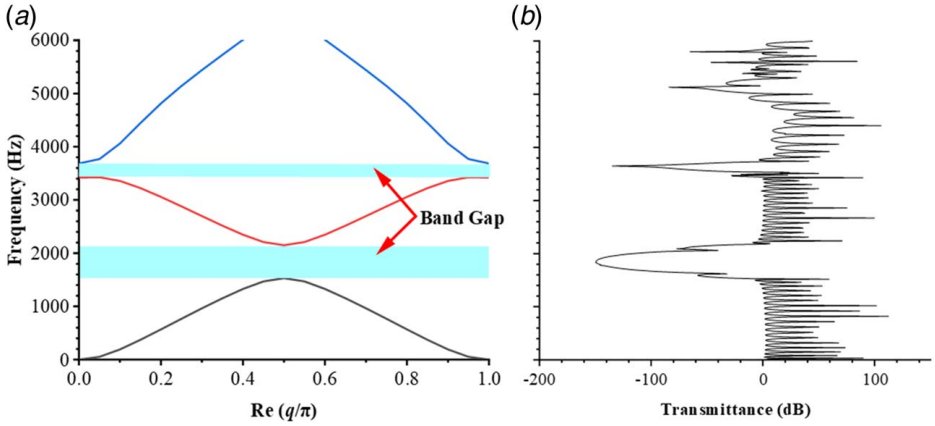

Fig. 7 (*a*) Band structure of the PCSB and (*b*) transmittance of the PCSB

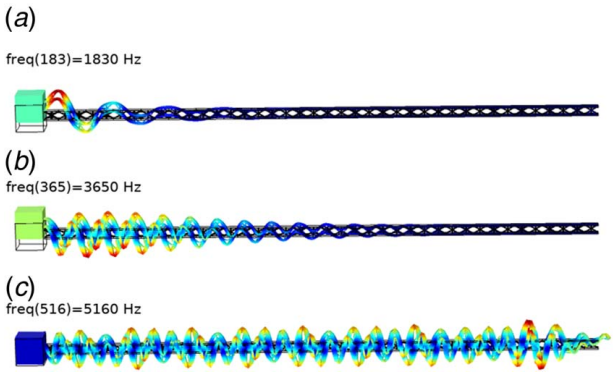

Fig. 8 Vibration modes of the PCSB under harmonic excitation: (*a*) within band gap (1830 Hz), (*b*) within band gap (3650 Hz), and (*c*) out of band gap (5160 Hz)

technology, it is fabricated. The complete experimental setup is shown in Fig. 11. One end of the PCSB is fixed on the mechanical shaker, while the other end is unconstrained. The mechanical shaker provides excitation at the clamping end in order to sweep the frequency, where the signal generator can determine the waveform, start and stop frequency, and sweeping time. An accelerometer is installed on the free side, and the acceleration change of the free side is recorded and displayed in the software as the vibration occurs.

The frequency range for the experiment is set to 0–1230 Hz, and the excitation waveform is a sinusoidal function. The absolute value of the acceleration is processed first, and the maximum value near the corresponding frequency point is the experimental data. The processed experimental results and the simulation results are depicted in Fig. 12. The band gaps of the PCSB are 427–630 and 1021–1169 Hz, and the band gaps obtained by COMSOL are 437–650 and 1017–1157 Hz, respectively. The relative error between the two methods could be acceptable (4.7% and 5.7%). Due to

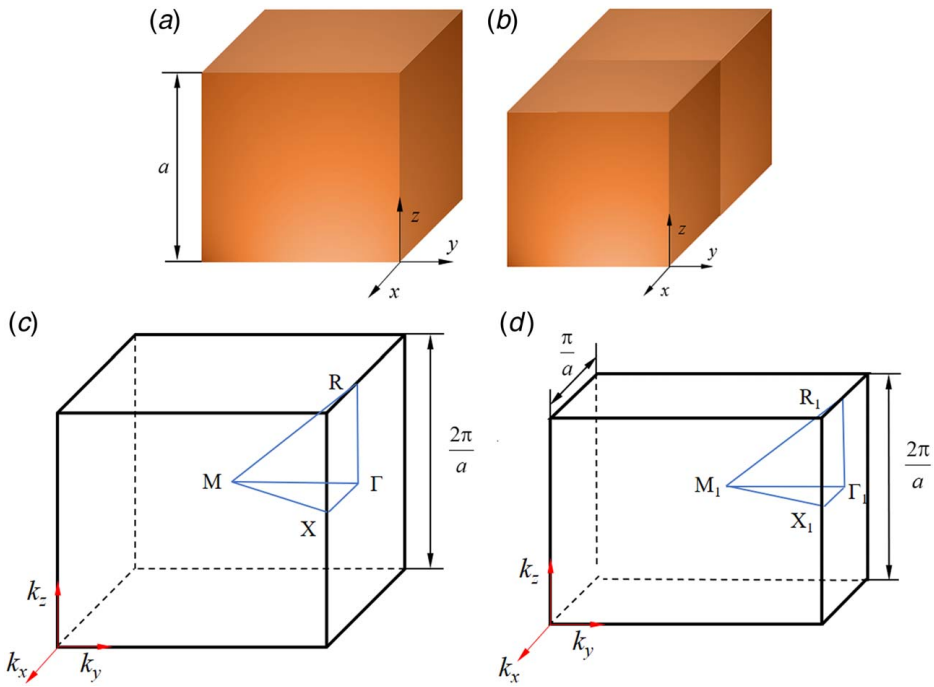

Fig. 9 (*a*) The simple cubic lattice, (*b*) the double-volume cell, (*c*) the inverse space of simple cubic lattice, and (*d*) the inverse space of the double-volume cell

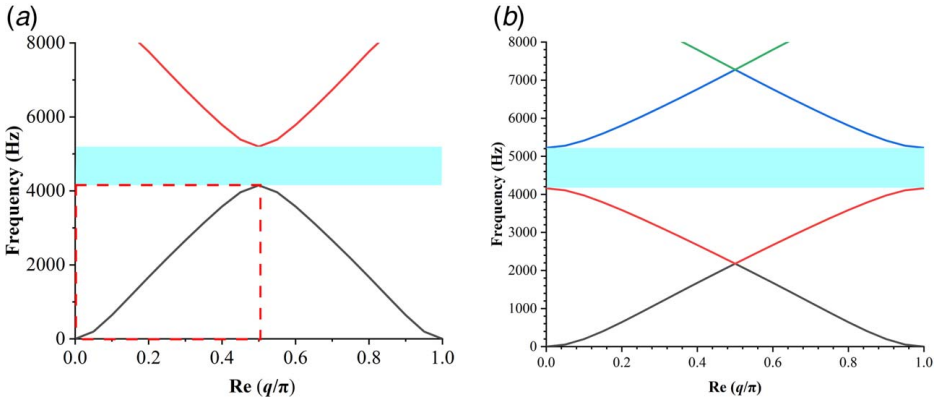

Fig. 10 (*a*) Band structure of the TSB unit cell and (*b*) band structure of the RVE with two identical TSB unit cells

Table 3 The geometric and material parameters of the PCSB

Length of beam (mm)	Clamping length (mm)	Periodicity	r_1 (mm)	r_2 (mm)	E (GPa)	ρ (kg/m^3)	ν
1700	100	8	5	2	3.5	1250	0.35

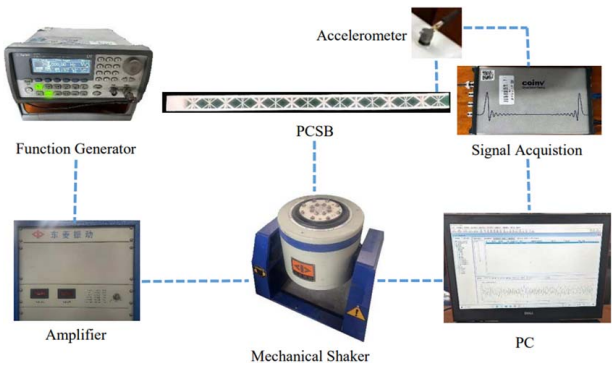

Fig. 11 Experimental setup for testing the sandwich beams

the defects of manufacturing and the error of the experimental process, there are some discrepancies in the experimental frequency response curve, while it barely makes a difference regarding the approximate position of the band gaps. In addition, the accelerometer also records non-transverse acceleration, which cannot also be ignored.

4 Parametric Study

The study in the previous section has proven that the PCSB can produce lower frequency band gaps and more band gaps than the TSB by opening up the folding points. To meet various design and optimization requirements, investigating the parameter sensitivity of the PCSB is necessary and of great importance. Hence, a parametric study is performed in this section. The PCSB's band gap properties are examined by varying the geometric parameters. The PCSB structure has many geometric parameters. Representative structural parameters, including the radius ratio ($\delta = r_2/r_1$), the inclination angles (α), and the core layer thickness (h_c), will be considered in this section.

4.1 Effect of Rod Radius Ratio. We first fix the inclination angles (α) at 30 deg and the core layer thickness (h_c) at 50 mm. By keeping $r_1 = 5$ mm, we then change the radius ratio (δ). In other words, r_2 varies and takes a series of values, 1–6 mm in the FE simulation. The transmittance calculation results of the PCSB are presented in Fig. 13. The band gaps are identified, and their ranges are listed in Table 4. As noted, when δ increases from 0.2 to 1.2 mm, the first two band gaps of PCSB move to the higher frequency. This result is similar to the phenomenon of the local resonant sandwich beam reported in Ref. [21]. The band gap frequency is related to the mass and stiffness. The increase of r_2 will increase the stiffness and mass of the PCSB. Since the maximum r_2 is only

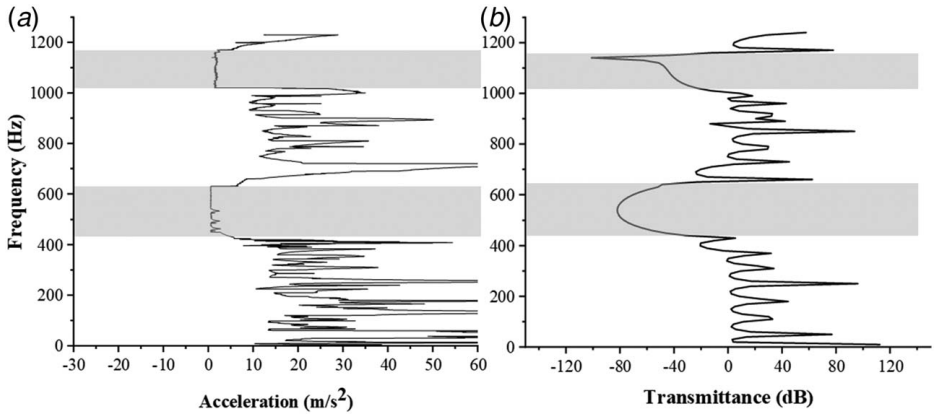

Fig. 12 (*a*) Experimental results and (*b*) simulation results

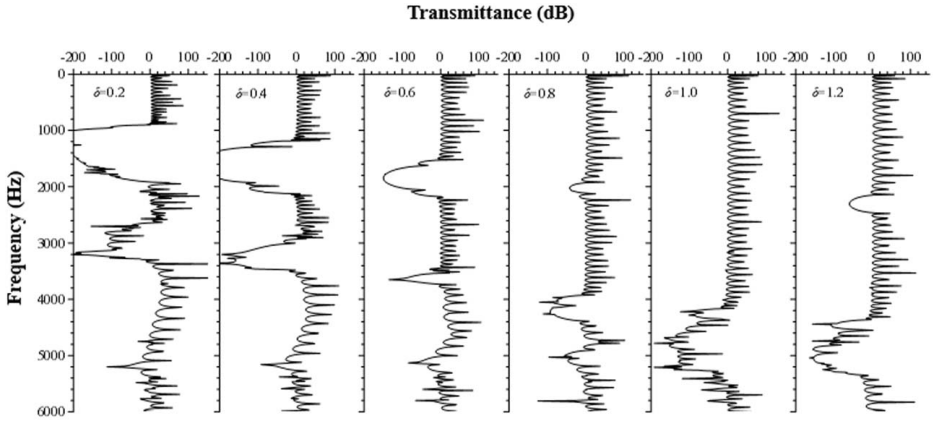

Fig. 13 Transmittances of the PCSB with various δ

Table 4 The frequency data of the PCSB with various δ

Δ	First band gap (Hz)	Bandwidth (Hz)	Second band gap (Hz)	Bandwidth (Hz)
0.2	901.60–1950.87	1049.27	2639.75–3256.76	617.01
0.4	1184.38–2107.54	923.16	2896.31–3445.74	549.43
0.6	1530.33–2149.04	618.71	3427.26–3685.86	258.60
0.8	1872.89–2175.98	303.09	3934.00–4339.23	405.23
1.0	–	–	4158.83–5223.69	1064.86
1.2	2166.84–2434.80	267.96	4354.81–5285.14	930.33

Table 5 The band gap information of the PCSB with various α

α (deg)	First band gap (Hz)	Bandwidth (Hz)	Second band gap (Hz)	Bandwidth (Hz)
30 deg	1531.35–2145.47	614.12	3430.54–3668.99	238.45
30.5 deg	1532.63–2136.24	603.61	3450.36–3632.12	181.76
31 deg	1532.47–2122.11	589.64	3466.89–3590.37	123.48
32 deg	1528.13–2094.23	566.10	3486.93–3510.24	23.31
32.5 deg	1525.59–2080.18	554.59	3472.06–3495.17	23.11
33 deg	1521.01–2063.81	542.80	3431.53–3497.00	65.47
35 deg	1498.31–1994.37	496.06	3277.20–3484.37	207.17
37.5 deg	1459.64–1904.46	444.82	3102.94–3418.37	315.43
40 deg	1414.73–1818.07	403.34	2952.14–3318.15	366.01
42.5 deg	1367.76–1736.65	368.89	2821.53–3201.72	380.19
45 deg	1319.72–1661.64	341.92	2709.99–3076.06	366.07
47.5 deg	1272.55–1593.84	321.29	2615.43–2950.13	334.70
50 deg	1226.04–1531.07	305.03	2533.97–2824.54	290.57

6 mm, the mass increase is negligible. Thus, the effect on the stiffness is relatively significant, and the stiffness increase will make the band gap frequency higher. This is because increasing r_2 reinforces the strength of the beam structure. Unsurprisingly, the structural frequencies, including the resonant frequencies and band gap frequency range, get higher. Besides, the first band gap becomes smaller while the second band gap becomes narrower at first, wider later, and narrower again. When $r_2 = r_1$, the folding point is closed, and two band gaps disappear. The obtained results are consistent with the band structure analysis of the TSB in Fig. 10(*b*). In general, when r_2 is set small, the first band gap becomes significantly broad. When $r_2 = r_1$, the width of the "second" band gap range reaches the maximum. The first band gap disappears in this case. Thus, to achieve effective suppression of low-frequency broadband vibration, a relatively small radius r_2 is recommended to be considered.

4.2 Effect of Rod Inclination Angle. In the second study, the inclination angle α is varied. Note that the inclination angle is determined by $L_1 = h_c/(2\tan\alpha)$. The band gap information of the PCSB with different inclination angles is collected in Table 5. As α increases from 30 deg to 50 deg, the first two band gaps shift toward the lower frequency, and this can be attributed to the reduction in the length of the supporting truss as α increases. Thus, the bending stiffness of the core layer decreases while the mass change is negligible. Consequently, the spectral response of the PCSB, including the resonant frequencies and band gap frequency range, shifts toward the lower frequency direction. Besides, it can be found that with the increase of α, the first band gap becomes smaller monotonically; the second band gap gets narrower, then wider, then narrower again. In summary, appropriately increasing the inclination angle α can lower band gap frequencies but may not be beneficial for achieving large band gaps.

Figure 14 demonstrates the impact of α on the band gaps of the PCSB. The second band gap is not easy to control since it is nearly closed over the range from 32 deg to 32.5 deg. Interestingly,

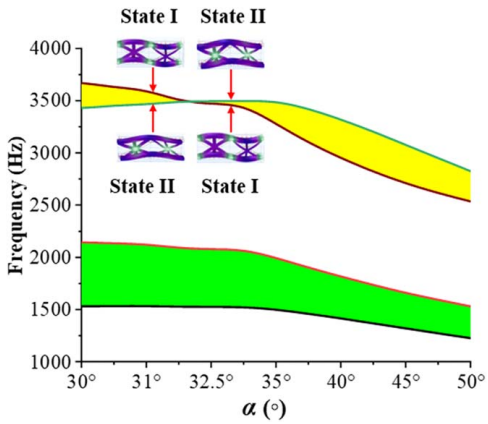

Fig. 14 Band gap evolution of the PCSB as α varies

polarization transition takes place within the PCSB's second band gap of the PCSB when α varies over 32 deg–32.5 deg. By plotting the edge modes, we can see that as α changes from 32 deg to 32.5 deg, the bottom and top edge modes of the RVE are swapped: the top edge mode shape changes from state I to state II, and the bottom edge mode shape changes from state II to state I. This band gap open-close-reopen process, together with the polarization transition behavior, is referred to as the band inversion phenomenon in many topological metamaterials [41–43]. Though it

Table 6 The frequency data of the PCSB with various h_c

h_c (mm)	First band gap (Hz)	Bandwidth (Hz)	Second band gap (Hz)	Bandwidth (Hz)
23.4	1244.90–1750.52	505.62	3377.41–3445.50	68.09
28.4	1244.90–1750.52	505.62	3377.41–3445.50	68.09
31.8	1338.20–1889.55	551.35	3465.27–3473.75	8.51
40.8	1439.91–2027.09	587.18	3476.34–3588.34	112.00
50.5	1530.33–2149.04	618.71	3419.87–3685.86	265.99
61.3	1616.72–2268.30	651.58	3440.24–3767.06	326.82
73.4	1677.83–2355.68	677.85	3459.07–3801.44	342.37
87.5	1714.12–2409.97	695.85	3429.90–3789.32	359.42

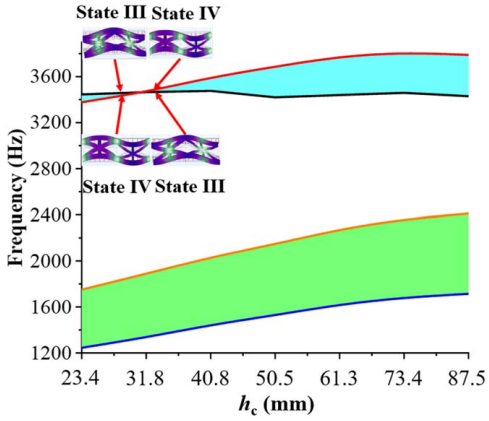

Fig. 15 Band gap evolution of the PCSB as h_c varies

brings no benefit for vibration attenuation, this unique phenomenon can be employed to design topological structures.

4.3 Effect of Core Layer Thickness. This subsection investigates the impact of h_c on the band gaps of the PCSB while keeping all other parameters fixed. In the study, we increased h_c from 23.4 to 87.5 mm. From the information offered in Table 6, increasing h_c shifts the first band gap toward the higher frequency direction and widens it. The increase of h_c in this section also only greatly influences the stiffness and has a minor effect on the mass. The stiffness increase moves the band gap toward a higher frequency. In this tuning process, the second band gap first shrinks to almost closed, then expands again. Similarly, the band gap open-close-reopen phenomenon occurs once more. Figure 15 graphically shows the process. The edge modes are examined again. We notice that the upper edge mode at $h_c = 28.4$ mm becomes similar to the lower edge mode at $h_c = 31.8$ mm. Meanwhile, the lower edge mode at $h_c = 28.4$ mm becomes like the upper edge mode at $h_c = 31.8$ mm. Therefore, tuning the core layer thickness provides another way to alter the topological properties of the PCSB and trigger topological interface states, which is out of the scope of this work. Back to the vibration attenuation topic, we know that increasing the core layer thickness within a reasonable range can indeed widen band gaps. However, one has to pay attention that this will also increase band gap frequencies, which is unfavorable for low-frequency applications.

5 Extension to Multi-folding Strategy

Suppose an RVE is composed of two identical unit cells, the band-folding phenomenon occurs, which is named first-folding here. Band-folding gives rise to folding points. Then, by introducing diversities between neighboring unit cells in the RVE, folding points are opened, and new band gaps are generated. This is the basic idea for widening band gaps in this study. On this basis, we propose to increase the folding order, i.e., the number of unit cells contained in the RVE of the PCSB. For example, an RVE with three unit cells corresponds to a second-folding PCSB; and an RVE with four unit cells corresponds to a third-folding PCSB. We expect to open more band gaps in the PCSB for extremely broadband vibration attenuation by introducing a multiple-folding mechanism.

For simplicity but without loss of generality, vibration band gap properties of second-folding and third-folding PCSBs are studied, in which PCSBs are composed of 20 RVEs. For the former one, the rod radii of the three unit cells in the RVE are 5, 3, and 5 mm, respectively; while for the latter one, the rod radii of the four unit cells in the RVE are 5, 4, 3, and 2 mm, respectively. The two models built in COMSOL are shown in Figs. 16(*a*) and 16(*b*), respectively.

Figures 17(*a*) and 17(*b*) show the band structures of the second-folding and third-folding PCSBs, respectively. It is seen that compared to the TSB and the first-folding PCSB studied in the previous sections, there appear more band gaps below 6000 Hz in the second-folding and third-folding PCSBs. Though the third-folding PCSB produces more band gaps than the second-folding model, the band gaps of the third-folding PCSB are much narrower than those of the second-folding PCSB. Hence, it is known that we cannot simply increase the folding order to widen band gaps. To truly realize broadband vibration attenuation, we also need to consider the band gap width. Just as the parametric analysis for the first-folding case, similar studies must be conducted for multi-folding models to confirm their actual band gaps.

Correspondingly, Figs. 17(*c*) and 17(*d*) demonstrate the transmittances of the second-folding and third-folding PCSBs. The transmittance results outcomes are highly consistent with the band structure analysis results. Compared to the results of the first-folding PCSB in Fig. 7(*b*), we notice more attenuation valleys on the transmittance curves of the second-folding and third-folding PCSBs. In addition to the widths and number of band gaps, we can also evaluate their actual attenuation abilities in the transmittance plot. For the valleys on the transmittance curve of the second-folding PCSB, their depths are much larger than those of the third-folding PCSB. In frank works, a deeper valley indicates a stronger vibration attenuation ability. Thus, we know that the second-folding PCSB can better mitigate the vibrations. This perspective echoes the previous statement that simply increasing the folding order may not benefit vibration attenuation. Again, we would like to emphasize that a parametric analysis or an optimization study is essential if one chooses to improve the vibration attenuation abilities of PCSB by using the multi-folding strategy. In other words, the structural parameters must be meticulously tuned to make good use of the multi-folding strategy.

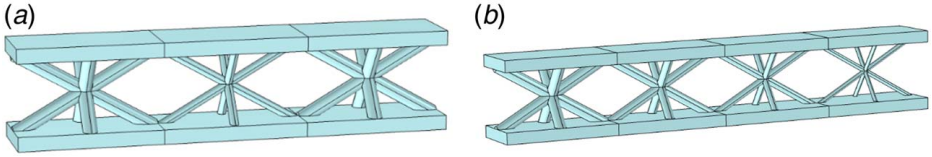

Fig. 16 The RVE of multi-folding PCSB: (*a*) second-folding model and (*b*) third-folding model

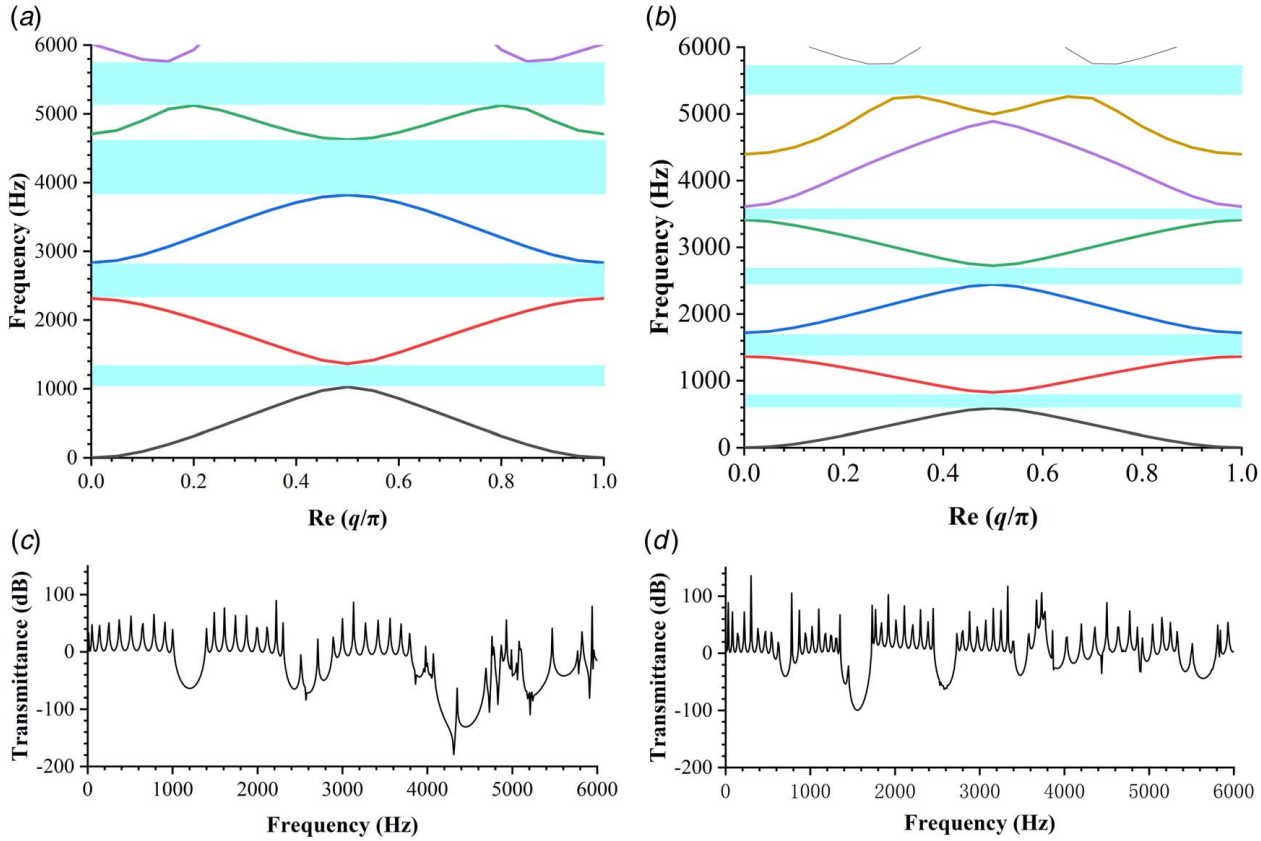

Fig. 17 (*a*) Band structure of the second-folding PCSB, (*b*) band structure of the third-folding PCSB, (*c*) transmittance of the second-folding PCSB, and (*d*) transmittance of the third-folding PCSB

6 Conclusion

A novel PCSB with an hourglass lattice truss core has been proposed in this study. Before building the PCSB model, an existing pyramidal truss core sandwich beam was established and analyzed. The results were compared with those in the literature to verify the modeling method. Subsequently, the band-folding effect and folding points are found in the band structure of the TSB. The spatial symmetry is destroyed by transforming the TSB to the PCSB, and the folding point is split. Compared with the TSB, the PCSB could produce two additional band gaps, indicating that broadband vibration suppression can be achieved. Furthermore, the transmittance response of the PCSB is calculated to verify the band gap prediction by the band structure analysis. For the experiment of the PCSB, PLA material and additive manufacturing technology are used, and the frequency sweep from 0 to 1230 Hz is basically consistent with the simulation. Based on the developed PCSB model, the effects of geometric parameters on the band gaps of the PCSB were investigated. The findings are summarized below:

- With the increase of the rod radius r_2, the first band gap moves to the high-frequency direction and gets narrower; the second band gap also shifts to the high-frequency direction, but its width first decreases, then increases, and finally decreases again.
- The increase of the core layer thickness h_c moves the first band gap to a higher frequency and widens it; while the second band gap first narrows down to almost closed, then widens again, and moves to a higher frequency first, then back to a lower frequency.
- A larger inclination angle α from 30 deg to 50 deg results in a smaller equivalent stiffness and shifts the first two band gaps to a lower frequency. The width of the first band gap becomes smaller, while the second band gap first narrows, then widens, and then narrows again.

In summary, the research shows that the rod radius, inclination angle, and core thickness significantly affect the structural stiffness, but the effect on the structural mass is limited. By following the above guidelines, one can tune the structural parameters to customize the band gaps of the PCSB. It is worth emphasizing that band inversion appeared in the process of varying α and h_c, resulting from the topological phase transition. This indicates that the current PCSB can be employed to design topological structures. Finally, higher-order band-folding PCSBs were explored. Second-folding and third-folding models were modeled and studied. It was revealed that increasing the folding order could open more band gaps. However, simply increasing the folding order may not help achieve wide band gaps and could weaken the vibration suppression ability. Structural parameters must be meticulously tuned to make good use of the multi-folding strategy.

Funding Data

- The National Natural Science Foundation of China (Grant Nos. 12102031 and 52305135).
- The Guangdong Provincial Key Lab of Integrated Communication, Sensing and Computation for Ubiquitous Internet of Things, the Hong Kong University of Science and Technology (Guangzhou).
- The State Key Laboratory of Structural Analysis for Industrial Equipment, Dalian University of Technology, China (GZ21114).
- Beijing University of Civil Engineering and Architecture 2023 Graduate Student Innovation Project (PG2023132).

Conflict of Interest

There are no conflicts of interest.

Data Availability Statement

The datasets generated and supporting the findings of this article are obtainable from the corresponding author upon reasonable request.

References

[1] Wang, J. F., Shi, C. Y., Yang, N., Sun, H. N., Liu, Y. Q., and Song, B. Y., 2018, "Strength, Stiffness, and Panel Peeling Strength of Carbon Fiber-Reinforced Composite Sandwich Structures With Aluminum Honeycomb Cores for Vehicle Body," Compos. Struct., **184**, pp. 1189–1196.

[2] Yang, W., Xiong, J., Feng, L. J., Pei, C., and Wu, L. Z., 2020, "Fabrication and Mechanical Properties of Three-Dimensional Enhanced Lattice Truss Sandwich Structures," J. Sandw. Struct. Mater., **22**(5), pp. 1594–1611.

[3] Harvey, D., and Hubert, P., 2020, "Extensions of the Coating Approach for Topology Optimization of Composite Sandwich Structures," Compos. Struct., **252**, p. 112682.

[4] Chai, Y. Y., Du, S. J., Li, F. M., and Zhang, C. Z., 2021, "Vibration Characteristics of Simply Supported Pyramidal Lattice Sandwich Plates on Elastic Foundation: Theory and Experiments," Thin-Walled Struct., **166**, p. 108116.

[5] Guo, Z. K., Hu, G. B., Jiang, J. C., Yu, L. D., Li, X., and Liang, J. R., 2021, "Theoretical and Experimental Study of the Vibration Dynamics of a 3D-Printed Sandwich Beam With an Hourglass Lattice Truss Core," Front. Mech. Eng., **7**, p. 651998.

[6] Zhang, Y. W., Li, Z., Xu, K. F., and Zang, J., 2021, "A Lattice Sandwich Structure With the Active Variable Stiffness Device Under Aerodynamical Condition," Aerosp. Sci. Technol., **116**, p. 106849.

[7] Bai, X. H., Zheng, Z. H., and Nakayama, A., 2019, "Heat Transfer Performance Analysis on Lattice Core Sandwich Panel Structures," Int. J. Heat Mass Transfer, **143**, p. 118525.

[8] Lee, P. V. S., Ngo, T. D., Imbalzano, G., and Tran, P., 2017, "Three-Dimensional Modelling of Auxetic Sandwich Panels for Localised Impact Resistance," J. Sandw. Struct. Mater., **19**(3), pp. 291–316.

[9] Rohini, R., and Bose, S., 2019, "Electrodeposited Carbon Fiber and Epoxy Based Sandwich Architectures Suppress Electromagnetic Radiation by Absorption," Compos. B: Eng., **161**, pp. 578–585.

[10] Guo, Z. K., Liu, C. C., and Li, F. M., 2019, "Vibration Analysis of Sandwich Plates With Lattice Truss Core," Mech. Adv. Mater. Struct., **26**(5), pp. 424–429.

[11] Wang, G., Yu, D. L., Wen, J. H., Liu, Y. Z., and Wen, X. S., 2004, "One-Dimensional Phononic Crystals With Locally Resonant Structures," Phys. Lett. A, **327**(5–6), pp. 512–521.

[12] Mead, D., and Markuš, Š., 1983, "Coupled Flexural-Longitudinal Wave Motion in a Periodic Beam," J. Sound Vib., **90**(1), pp. 1–24.

[13] Wu, Z., Li, F., and Zhang, C., 2018, "Band-Gap Analysis of a Novel Lattice With a Hierarchical Periodicity Using the Spectral Element Method," J. Sound Vib., **421**, pp. 246–260.

[14] Hu, G., Tang, L., and Das, R., 2018, "Internally Coupled Metamaterial Beam for Simultaneous Vibration Suppression and Low Frequency Energy Harvesting," J. Appl. Phys., **123**(5), p. 055107.

[15] Liu, L., and Hussein, M. I., 2012, "Wave Motion in Periodic Flexural Beams and Characterization of the Transition Between Bragg Sattering and Local Resonance," ASME J. Appl. Mech., **79**(1), p. 011003.

[16] Cai, C. Q., Zhou, J. X., Wang, K., Pan, H. B., Tan, D. G., Xu, D. L., and Wen, G. L., 2022, "Flexural Wave Attenuation by Metamaterial Beam With Compliant Quasi-Zero-Stiffness Resonators," Mech. Syst. Signal Process., **174**, p. 109119.

[17] Hu, G. B., Lan, C. B., Tang, L. H., and Yang, Y. W., 2022, "Local Resonator Stimulated Polarization Transition in Metamaterials and the Formation of Topological Interface States," Mech. Syst. Signal Process., **165**, p. 108388.

[18] Nassar, H., Chen, H., Norris, A., Haberman, M., and Huang, G. L., 2017, "Non-Reciprocal Wave Propagation in Modulated Elastic Metamaterials," Proc. R. Soc. A: Math. Phys. Eng. Sci., **473**(2202), p. 20170188.

[19] Chen, J. S., and Sun, C. T., 2011, "Dynamic Behavior of a Sandwich Beam With Internal Resonators," J. Sandw. Struct. Mater., **13**(4), pp. 391–408.

[20] Sharma, B., and Sun, T. C., 2016, "Local Resonance and Bragg Bandgaps in Sandwich Beams Containing Periodically Inserted Resonators," J. Sound Vib., **364**, pp. 133–146.

[21] Guo, Z. K., Hu, G. B., Sorokin, V., Tang, L. H., Yang, X. D., and Zhang, J., 2021, "Low-Frequency Flexural Wave Attenuation in Metamaterial Sandwich Beam With Hourglass Lattice Truss Core," Wave Motion, **104**, p. 102750.

[22] Li, H., Hu, Y. B., Huang, H. Y., Chen, J. L., Zhao, M. Y., and Li, B., 2021, "Broadband Low-Frequency Vibration Attenuation in 3D Printed Composite Meta-Lattice Sandwich Structures," Compos. B: Eng., **215**, p. 108772.

[23] Guo, J. J., Li, Y. Q., Xiao, Y., Fan, Y. L., Yu, D. L., and Wen, J. H., 2022, "Multiscale Modeling and Design of Lattice Truss Core Sandwich Metastructures for Broadband Low-Frequency Vibration Reduction," Compos. Struct., **289**, p. 115463.

[24] An, X. Y., Yuan, X. F., Hou, X. X., and Fan, H. L., 2023, "Low Frequency Vibration Attenuation of Meta-Orthogrid Sandwich Panel With High Load-Bearing Capacity," Compos. Struct., **305**, p. 116560.

[25] Cai, C. Q., Zhou, J. X., Wu, L. C., Wang, K., Xu, D. L., and Ouyang, H. J., 2020, "Design and Numerical Validation of Quasi-Zero-Stiffness Metamaterials for Very Low-Frequency Band Gaps," Compos. Struct., **236**, p. 111862.

[26] Fang, X., Wen, J. H., Bonello, B., Yin, J. F., and Yu, D. L., 2017, "Ultra-Low and Ultra-Broad-Band Nonlinear Acoustic Metamaterials," Nat. Commun., **8**(1), p. 1288.

[27] Xue, Y., Li, J. Q., Wang, Y., and Li, F. M., 2021, "Tunable Nonlinear Band Gaps in a Sandwich-Like Meta-Plate," Nonlinear Dyn., **106**, pp. 2841–2857.

[28] Li, J., Fan, X., and Li, F., 2020, "Numerical and Experimental Study of a Sandwich-Like Metamaterial Plate for Vibration Suppression," Compos. Struct., **238**, p. 111969.

[29] Li, H., Li, Y. L., and Liu, X., 2023, "Double-Beam Metastructure With Inertially Amplified Resonators for Flexural Wave Attenuation," Eur. J. Mech. A/Solids., **97**, p. 104794.

[30] He, F. Y., Shi, Z. Y., Qian, D. H., Tu, J., and Chen, M. L., 2022, "Flexural Wave Bandgap Properties in Metamaterial Dual-Beam Structure," Phys. Lett. A, **429**, p. 127950.

[31] Guo, Z. K., Hu, G., Sorokin, V., Yang, Y., and Tang, L., 2021, "Sound Transmission Through Sandwich Plate With Hourglass Lattice Truss Core," J. Sandw. Struct. Mater., **23**(6), pp. 1902–1928.

[32] Feng, L. J., Wei, G. T., Yu, G. C., and Wu, L. Z., 2019, "Underwater Blast Behaviors of Enhanced Lattice Truss Sandwich Panels," Int. J. Mech. Sci., **150**, pp. 238–246.

[33] Muhammad, Zhou, W. J., and Lim, C. W., 2019, "Topological Edge Modeling and Localization of Protected Interface Modes in 1D Phononic Crystals for Longitudinal and Bending Elastic Waves," Int. J. Mech. Sci., **159**, pp. 359–372.

[34] Zhang, H. B., Liu, B. L., Zhang, X. L., Wu, Q. Q., and Wang, X. G., 2019, "Zone Folding Induced Tunable Topological Interface States in One-Dimensional Phononic Crystal Plates," Phys. Lett. A, **383**(23), pp. 2797–2801.

[35] Lou, J., Wang, B., Ma, L., and Wu, L. Z., 2013, "Free Vibration Analysis of Lattice Sandwich Beams Under Several Typical Boundary Conditions," Acta Mech. Sol. Sin., **26**(5), pp. 458–467.

[36] Li, Z. Y., Ma, T. X., Wang, Y. Z., Li, F. M., and Zhang, C. Z., 2020, "Vibration Isolation by Novel Meta-Design of Pyramid-Core Lattice Sandwich Structures," J. Sound Vib., **480**, p. 115377.

[37] Ashcroft, N. W., and Mermin, N. D., 2022, *Solid State Physics*, Cengage Learning, Orlando, FL.

[38] Indaleeb, M. M., Ahmed, H., Saadatzi, M., and Banerjee, S., 2020, "Deaf Band-Based Prediction of Dirac Cone in Acoustic Metamaterials," J. Appl. Phys., **127**(6), p. 064903.

[39] Indaleeb, M. M., Banerjee, S., Ahmed, H., Saadatzi, M., and Ahmed, R., 2019, "Deaf Band Based Engineered Dirac Cone in a Periodic Acoustic Metamaterial: A Numerical and Experimental Study," Phys. Rev. B, **99**(2), p. 024311.

[40] He, C., Lai, H.-S., He, B., Yu, S.-Y., Xu, X., Lu, M.-H., and Chen, Y.-F., 2020, "Acoustic Analogues of Three-Dimensional Topological Insulators," Nat. Commun., **11**(1), p. 2318.

[41] Ni, A. C., and Shi, Z. F., 2023, "Topological Metamaterial Plates: Numerical Investigation, Experimental Validation and Applications," Eng. Struct., **275**, p. 115288.

[42] Chen, Z., Zhou, W., and Lim, C., 2021, "Tunable Frequency Response of Topologically Protected Interface Modes for Membrane-Type Metamaterials Via Voltage Control," J. Sound Vib., **494**, p. 115870.

[43] Yu, D. W., Hu, G. B., Guo, Z. K., Hong, J., and Yang, Y. W., 2023, "Topological Interface State Formation in an Hourglass Lattice Sandwich Meta-Structure," Int. J. Mech. Sci., **246**, p. 108170.